Comput Mech (2012) 49:735–747
DOI 10.1007/s00466-012-0704-z

ORIGINAL PAPER

An abstract framework for a priori estimates for contact problems in 3D with quadratic finite elements

B. I. Wohlmuth · A. Popp · M. W. Gee · W. A. Wall

Received: 31 October 2011 / Accepted: 20 March 2012 / Published online: 11 April 2012

Abstract In this paper, a variationally consistent contact formulation is considered and we provide an abstract framework for the a priori error analysis in the special case of frictionless contact and small deformations. Special emphasis is put on quadratic mortar finite element methods. It is shown that under quite weak assumptions on the Lagrange multiplier space $\mathcal{O}(h^{t-1})$, $2 < t < \frac{5}{2}$, a priori results in the H^1-norm for the error in the displacement and in the $H^{-1/2}$-norm for the error in the surface traction can be established provided that the solution is regular enough. We discuss several choices of Lagrange multipliers ranging from the standard lowest order conforming finite elements to locally defined biorthogonal basis functions. The crucial property for the analysis is that the basis functions have a local positive mean value. Numerical results are exemplarily presented for one particular choice of biorthogonal (i.e. dual) basis functions and also comprise the case of finite deformation contact.

Keywords Mortar finite element methods · Lagrange multipliers · Contact problems · A priori error analysis

B. I. Wohlmuth
Institute for Numerical Mathematics, Technische Universität München, Boltzmannstrasse 3, 85748 Garching, Germany
e-mail: wohlmuth@ma.tum.de

A. Popp (✉) · W. A. Wall
Institute for Computational Mechanics, Technische Universität München, Boltzmannstrasse 15, 85748 Garching, Germany
e-mail: popp@lnm.mw.tum.de

M. W. Gee
Mechanics and High Performance Computing Group, Technische Universität München, Boltzmannstrasse 15, 85748 Garching, Germany
e-mail: gee@tum.de

1 Introduction

In many engineering problems, contact between elastic bodies plays a crucial role. Although early theoretical results go back to Hertz [11], the numerical simulation is still challenging and many theoretical questions remain open. There are several monographs on contact mechanics such as [5,16,17]. More recent existence and uniqueness results can be found in [4,9] and numerical simulation techniques are discussed in [18,32,33]. One of the main challenges relates to the fact that the transition between contact and non-contact is a priori not known and is characterized by a change in the type of the boundary condition possibly resulting in a solution of reduced regularity. Although quadratic finite elements offer several appealing features for contact analysis, such as an improved approximation of curved surfaces, mortar methods for 3D contact have so far mainly been analyzed and developed in the context of first-order interpolation. In contrast, the present contribution aims at establishing an abstract framework for a priori estimates for 3D contact problems with *quadratic* finite elements and at validating the obtained theoretical results with meaningful numerical examples.

The rest of the paper is organized as follows: In Sect. 2, we introduce the problem setting and its weak formulation. The non-penetration condition and Coulomb's friction law result in a variational inequality with a solution dependent convex cone as solution space for the surface traction. The discretization in terms of second order finite elements for the displacement is considered in Sect. 3. In Sect. 4, the main theoretical results can be found. We provide an abstract framework such that $\mathcal{O}(h^{t-1})$, $2 < t < \frac{5}{2}$, a priori results in the H^1-norm for the error in the displacement and in the $H^{-1/2}$-norm for the error in the surface traction can be established provided that the solution is regular enough. To do so, easy to verify assump-

tions on the Lagrange multiplier basis functions have to be imposed. We recall in Sect. 5 some of the choices for the Lagrange multipliers which can be found in the literature and show that all of them satisfy our assumptions. Finally in Sect. 6, numerical results are presented showing higher order accuracy of the quadratic approach compared to the linear discretization and also illustrating the flexibility of the presented scheme in the context of finite deformations.

2 Problem setting

For the sake of simplicity, we restrict the presentation to the simple case of a contact problem with small deformations here. Due to this assumption, the infinitesimal strain $\boldsymbol{\epsilon}(\mathbf{u}) := \frac{1}{2}(\nabla\mathbf{u} + \nabla\mathbf{u}^T)$ and the Cauchy stress $\boldsymbol{\sigma}(\mathbf{u}) := \mathcal{C}\boldsymbol{\epsilon}(\mathbf{u})$ can be used in the weak variational formulation, and the reference configuration can be identified with the current configuration. We refer to [7,23,24,26–28] for the more general finite deformation case. Let the open sets $\Omega^{\mathrm{m}}, \Omega^{\mathrm{s}} \subset \mathbb{R}^3$ represent two bodies in the reference configuration. The boundaries $\partial\Omega^l, l \in \{\mathrm{m}, \mathrm{s}\}$, are decomposed into three disjoint boundary sets Γ^l_{D}, Γ^l_{N} and Γ^l_{c}, where Γ^l_{D} stands for the non-trivial Dirichlet boundary part, Γ^l_{N} is the Neumann boundary, and Γ^l_{c} represents the potential contact surface.

The boundary value problem on $\Omega^l, l \in \{\mathrm{m}, \mathrm{s}\}$, of quasi-static small deformation elasticity reads as follows:

$$\begin{aligned} \mathrm{div}\boldsymbol{\sigma}^l + \mathbf{b}^l &= \mathbf{0}, && \text{in } \Omega^l \times (0,T), \\ \mathbf{u}^l &= \mathbf{u}^l_{\mathrm{D}}, && \text{on } \Gamma^l_{\mathrm{D}} \times (0,T), \\ \boldsymbol{\sigma}^l\mathbf{n}^l &= \mathbf{t}^l, && \text{on } \Gamma^l_{\mathrm{N}} \times (0,T), \end{aligned} \tag{1}$$

where $t \in [0,T]$ plays the role of a pseudo-time and $\mathbf{n}^l$ is the outer unit normal. The prescribed displacements on the Dirichlet boundary are given by $\mathbf{u}^l_{\mathrm{D}}$ and without loss of generality we assume $\mathbf{u}^l_{\mathrm{D}} = \mathbf{0}$. The Neumann data is denoted by $\mathbf{t}^l$, and $\mathbf{b}^l$ stands for a body force. In order to obtain a well-posed coupled system, the two bodies have to be in equilibrium, and we have to specify the conditions for non-penetration and friction. To do so, we use the linearized gap function $g_n \in H^{1/2}(\Gamma^{\mathrm{s}}_{\mathrm{c}})$ and introduce the negative surface traction $\boldsymbol{\lambda}$ on $\Gamma^{\mathrm{s}}_{\mathrm{c}}$ by $\boldsymbol{\lambda} := -\boldsymbol{\sigma}^{\mathrm{s}}\mathbf{n}^{\mathrm{s}}$. Then, the linearized non-penetration condition in normal direction reads as

$$[u_n] \le g_n\,, \quad \lambda_n \ge 0\,, \quad \lambda_n([u_n] - g_n) = 0\,, \tag{2}$$

where $\lambda_n := \boldsymbol{\lambda}\mathbf{n}^{\mathrm{s}}$ is the normal component of the surface stress, and $[u_n] := (\mathbf{u}^{\mathrm{s}} - \mathbf{u}^{\mathrm{m}} \circ \chi)\mathbf{n}^{\mathrm{s}}$ is the jump of the mapped boundary displacements. Here $\chi(\cdot)$ denotes a suitable mapping from $\Gamma^{\mathrm{s}}_{\mathrm{s}}$ onto $\Gamma^{\mathrm{m}}_{\mathrm{c}}$. In addition to (2), we have to satisfy Coulomb's law in tangential direction:

$$\|\boldsymbol{\lambda}_t\| \le \nu\lambda_n, \quad [\dot{\mathbf{u}}_t]\boldsymbol{\lambda}_t - \nu\lambda_n\|[\dot{\mathbf{u}}_t]\| = 0\,, \tag{3}$$

where the tangential components are defined by $\boldsymbol{\lambda}_t := \boldsymbol{\lambda} - \lambda_n\mathbf{n}^{\mathrm{s}}$ and $[\mathbf{u}_t] := [\mathbf{u}] - [u_n]\mathbf{n}^{\mathrm{s}}$, $[\mathbf{u}] := \mathbf{u}^{\mathrm{s}} - \mathbf{u}^{\mathrm{m}} \circ \chi$, $\nu \ge 0$ is the friction coefficient, and $\|\cdot\|$ stands for the Euclidean norm.

For further details on contact kinematics and frictional sliding the interested reader is referred to [17,18,32]. To start the derivation of a weak formulation of (1), we define $\mathbf{V} := \mathbf{V}^{\mathrm{m}} \times \mathbf{V}^{\mathrm{s}}$, $\mathbf{V}^{\mathrm{m}} := (V^{\mathrm{m}})^3$, $\mathbf{V}^{\mathrm{s}} := (V^{\mathrm{s}})^3$ with

$$V^l := \left\{ v^l \in H^1(\Omega^l),\ |\ v^l = 0 \ \text{ on } \Gamma^l_{\mathrm{D}} \right\}, \quad l \in \{\mathrm{m}, \mathrm{s}\}.$$

For simplicity of notation, we use the same symbol for vectorial as for scalar spaces and operators but use a bold font for vectorial spaces, i.e., V denotes a scalar valued space whereas $\mathbf{V}$ stands for the vectorial version. In addition to the displacement $\mathbf{u} = (\mathbf{u}^{\mathrm{m}}, \mathbf{u}^{\mathrm{s}})$, we use the negative surface traction $\boldsymbol{\lambda}$ on $\Gamma^{\mathrm{s}}_{\mathrm{c}}$ as additional unknown. Thus we have to specify a suitable set for the Lagrange multiplier $\boldsymbol{\lambda}$. Let $\mathbf{M}$ be the dual space of the trace space $\mathbf{W}$ of $\mathbf{V}^{\mathrm{s}}$ restricted to $\Gamma^{\mathrm{s}}_{\mathrm{c}}$. Then we define the non-empty closed convex cone $\mathbf{M}(\boldsymbol{\lambda})$ by

$$\begin{aligned} \mathbf{M}(\boldsymbol{\lambda}) := \{\boldsymbol{\mu} \in \mathbf{M} \mid \langle \boldsymbol{\mu}, \mathbf{v}\rangle_{\Gamma^{\mathrm{s}}_{\mathrm{c}}} \le \langle \nu\lambda_n, \|\mathbf{v}_t\|\rangle_{\Gamma^{\mathrm{s}}_{\mathrm{c}}}, \\ \text{for } \mathbf{v} \in \mathbf{W} \text{ with } -v_n \in W^+\}, \end{aligned} \tag{4}$$

where $\langle\cdot,\cdot\rangle_{\Gamma^{\mathrm{s}}_{\mathrm{c}}}$ stands for the scalar or vectorial valued duality pairing between $H^{-1/2}$ and $H^{1/2}$ on $\Gamma^{\mathrm{s}}_{\mathrm{c}}$. Moreover, W^+ is a closed non-empty convex cone being defined by $W^+ := \{w \in W, w \ge 0\}$, where W is the trace space of V^{s} restricted to $\Gamma^{\mathrm{s}}_{\mathrm{c}}$. We note that the definition (4) of the solution cone for the Lagrange multiplier satisfies the condition on $\boldsymbol{\lambda}$ of the friction law weakly. In terms of these preliminary definitions, the weak saddle-point formulation of a quasi-static Coulomb friction problem between two linearly elastic bodies reads as: Find $(\mathbf{u}, \boldsymbol{\lambda}) \in \mathbf{V} \times \mathbf{M}(\boldsymbol{\lambda})$ such that for all $\mathbf{v} \in \mathbf{V}$ and $\boldsymbol{\mu} \in \mathbf{M}(\boldsymbol{\lambda})$

$$a(\mathbf{u}, \mathbf{v}) + b_n(\boldsymbol{\lambda}, \mathbf{v}) + b_t(\boldsymbol{\lambda}, \mathbf{v}) = f(\mathbf{v}), \tag{5a}$$

$$b_n(\boldsymbol{\mu} - \boldsymbol{\lambda}, \mathbf{u}) + b_t(\boldsymbol{\mu} - \boldsymbol{\lambda}, \dot{\mathbf{u}}) \le g(\boldsymbol{\mu} - \boldsymbol{\lambda}), \tag{5b}$$

where the bilinear forms and the linear form are given for $\mathbf{v}, \mathbf{w} \in \mathbf{V}$ and $\boldsymbol{\mu} \in \mathbf{M}$ by

$$a(\mathbf{w}, \mathbf{v}) := \sum_{i=\mathrm{m,s}} \int_{\Omega^i} \boldsymbol{\sigma}(\mathbf{w}) : \boldsymbol{\epsilon}(\mathbf{v}),$$

$$b_n(\boldsymbol{\mu}, \mathbf{w}) := \langle \mu_n, [w_n]\rangle_{\Gamma^{\mathrm{s}}_{\mathrm{c}}}, \quad b_t(\boldsymbol{\mu}, \mathbf{w}) := \langle \boldsymbol{\mu}_t, [\mathbf{w}_t]\rangle_{\Gamma^{\mathrm{s}}_{\mathrm{c}}},$$

$$f(\mathbf{w}) := \sum_{i=\mathrm{m,s}} \int_{\Omega^i} \mathbf{b}^i\mathbf{w} + \int_{\Gamma^i_{\mathrm{N}}} \mathbf{t}^i\mathbf{w},$$

$$g(\boldsymbol{\mu}) := \langle \mu_n, g_n\rangle_{\Gamma^{\mathrm{s}}_{\mathrm{c}}}.$$

We note that (5a) corresponds to the equilibrium and that (5b) reflects in a weak form the non-penetration condition

(2) and the friction law (3). It is easy to see that $b_n(\boldsymbol{\mu}, \mathbf{w}) + b_t(\boldsymbol{\mu}, \mathbf{w}) = \langle \boldsymbol{\mu}, [\mathbf{w}] \rangle_{\Gamma_c^s}$. Moreover, setting $\boldsymbol{\mu} = \boldsymbol{\lambda} \pm \lambda_n \mathbf{n}^s$ yields the complementarity $b_n(\boldsymbol{\lambda}, \mathbf{u}) = g(\boldsymbol{\lambda})$ in normal direction.

3 Second order finite elements

The saddle point problem (5) in terms of the displacement and the contact traction is the starting point for the discrete formulation. For the displacement we use standard conforming finite elements of second order on each subdomain $\mathbf{V}_h := \mathbf{V}_h^m \times \mathbf{V}_h^s$ with homogeneous Dirichlet boundary conditions on the discrete approximation of the Dirichlet part, i.e., continuous element-wise quadratic elements on simplicials and 27-node or 20-node elements in 3D on hexahedrals. The regularity of the solution is assumed to be such that $\mathbf{u} \in \mathbf{H}^t(\Omega^m) \times \mathbf{H}^t(\Omega^s)$, $2 < t < \frac{5}{2}$, and we note that for $1 \leq t \leq 2$ no qualitative gain from the use of quadratic elements can be expected. We refer to [2,12,13] for an a priori analysis in the 2D setting of special Lagrange multiplier choices. Here, we focus on an abstract formulation and to the 3D situation. We also introduce $W_h^{(1)}$, which stands for the trace space of lowest order conforming finite elements on the slave side restricted to the discrete contact boundary part. Associated with $W_h^{(1)}$ are the nodal basis functions $N_l^{(1)}$.

The regularity of the solution compared to a linear elasticity problem with homogeneous Dirichlet boundary conditions on a convex domain and smooth right hand side is reduced due to the fact that the inequality constraint generates a free boundary which marks the separation between Dirichlet and Neumann boundary type conditions. Due to the sign condition in (2), the first singular term in a Signorini type problem does not occur and the second expansion term gives a regularity of $H^{\frac{5}{2}-\epsilon}$ for all $\epsilon > 0$, see [20]. These observations motivate our interest in quadratic finite elements and a priori estimates of order $t - 1$ with $2 < t < \frac{5}{2}$.

We do not require that the slave and the master subdomain are exactly represented by the elements, i.e., the union of all elements on the master side Ω_h^m and on the slave side Ω_h^s approximate Ω^m and Ω^s, respectively. The scalar and vector valued H^1-product space on $\Omega_h := \Omega_h^m \cup \Omega_h^s$ is denoted by $H^1(\Omega_h) := H^1(\Omega_h^m) \times H^1(\Omega_h^s)$ and $\mathbf{H}^1(\Omega_h) := \mathbf{H}^1(\Omega_h^m) \times \mathbf{H}^1(\Omega_h^s)$, respectively.

To obtain a well-defined primal-dual problem in the discrete setting, we have to specify in addition $\mathbf{M}_h := (M_h)^3$ and the discrete cone $\mathbf{M}_h(\boldsymbol{\lambda}_h)$. Let $\{\Psi_j\}_{j=1,\dots m_h^s}$ be a basis of M_h associated with some set of nodes $\{x_j\}_{j=1,\dots m_h^s}$ on $\Gamma_{c;h}^s$, and assume that each $\boldsymbol{\mu} \in \mathbf{M}_h$ can be uniquely written as $\boldsymbol{\mu} = \sum_{i=1}^{m_h^s} \boldsymbol{\beta}_i \Psi_i$, $\boldsymbol{\beta}_i \in \mathbb{R}^3$, then we set

$$\mathbf{M}_h(\boldsymbol{\lambda}_h) := \{\boldsymbol{\mu} \in \mathbf{M}_h, \beta_i^n \geq 0, \|\boldsymbol{\beta}_i^{\mathbf{t}}\| \leq \nu \beta_i^n, \forall i = 1\}, \tag{6}$$

where $\mathbf{n}_i$ is an approximation of the outer unit normal at the node x_i and $\beta_i^n := \boldsymbol{\beta}_i \mathbf{n}_i$, $\boldsymbol{\beta}_i^{\mathbf{t}} := \boldsymbol{\beta}_i - \beta_i^n \mathbf{n}_i$. We point out that the choice of the basis $\{\Psi_j\}_{j=1}^{m_h^s}$ plays an important role for the definition of $\mathbf{M}_h(\boldsymbol{\lambda}_h)$. Moreover, (6) does not satisfy Coulomb's law in a strong form but only in a discrete sense.

Here we focus on the space discretization and thus for simplicity of presentation, we replace from now on $\dot{\mathbf{u}}$ in (5) by the increment $\Delta\mathbf{u}$. For convenience of notation, we restrict ourselves to the first incremental step with $\Delta\mathbf{u}$ being equal to $\mathbf{u}$. Then the weak formulation in its discrete version reads: Find $(\mathbf{u}_h, \boldsymbol{\lambda}_h) \in \mathbf{V}_h \times \mathbf{M}_h(\boldsymbol{\lambda}_h)$ such that for $\mathbf{v}_h \in \mathbf{V}_h$ and $\boldsymbol{\mu}_h \in \mathbf{M}_h(\boldsymbol{\lambda}_h)$, we have

$$a_h(\mathbf{u}_h, \mathbf{v}_h) + b_h(\boldsymbol{\lambda}_h, \mathbf{v}_h) = f_h(\mathbf{v}_h), \tag{7a}$$

$$b_h(\boldsymbol{\mu}_h - \boldsymbol{\lambda}_h, \mathbf{u}_h) \leq g_h(\boldsymbol{\mu}_h - \boldsymbol{\lambda}_h), \tag{7b}$$

where the bilinear forms and the linear forms are given for $\mathbf{v}, \mathbf{w} \in \mathbf{V}_h$ and $\boldsymbol{\mu} \in \mathbf{M}_h$ by

$$a_h(\mathbf{w}, \mathbf{v}) := \sum_{i=m,s} \int_{\Omega_h^i} \boldsymbol{\sigma}(\mathbf{w}) : \boldsymbol{\epsilon}(\mathbf{v}),$$

$$b_h(\boldsymbol{\mu}, \mathbf{w}) := \int_{\Gamma_{c;h}^s} \boldsymbol{\mu}_h [\mathbf{w}]_h,$$

$$f_h(\mathbf{w}) := \sum_{i=m,s} \int_{\Omega_h^i} \mathbf{b}^i \mathbf{w} + \int_{\Gamma_{N;h}^i} \mathbf{t}^i \mathbf{w},$$

$$g_h(\boldsymbol{\mu}) := \int_{\Gamma_{c;h}^s} \boldsymbol{\mu}_{h;n} g_h, \quad \boldsymbol{\mu}_{h;n} := \sum_{i=1}^{m_h^s} \beta_i^n \Psi_i$$

where the discrete jump is defined as $[\mathbf{w}]_h := \mathbf{w}|_{\Gamma_{c;h}^s} - \mathbf{w}|_{\Gamma_{c;h}^m} \circ \chi_h^{m,s}$, and $\chi_h^{m,s}$ is a suitable mapping from $\Gamma_{c;h}^s$ onto $\Gamma_{c;h}^m$, see also [6] for a rigorous analysis in 2D and [25,26] for the element-wise construction of such a mapping. The resulting solution algorithm employed here is based on a reformulation of the contact constraints within nonlinear complementarity (NCP) functions and a subsequent application of semismooth Newton methods, as presented in detail in [1,8,15,23]. It is well-known that Coulomb friction adds significant theoretical complexity to the contact problem as compared with the frictionless case. In certain situations, questions concerning existence and uniqueness of frictional solutions are still unanswered or yield unsatisfactory results, see e.g. [4] for a comprehensive overview.

Thus, the following investigations on a priori error bounds as well as the numerical results in Sect. 6 will focus exclusively on the frictionless case. Nevertheless, it should be pointed out that, albeit such difficulties, the algorithmic treatment of Coulomb friction can readily be achieved within the

same framework established for the contact constraints in normal direction, see e.g. our recent contributions [7,14,31].

4 A priori error bounds

For the a priori analysis in the H^1-norm for the error in the displacement and in the $H^{-1/2}$-norm for the error in the surface traction, we restrict ourselves to the simplest case of a contact problem with no friction and assume that $\Gamma_c = \Gamma^s_{c;h} = \Gamma^m_{c;h}$ with a constant normal, i.e., $g_n = 0$ and $\mathbf{n}$ is independent of the position on Γ_c. No friction can be regarded as a special case of Coulomb's law with $\nu = 0$, and thus we obtain from (3) that $\boldsymbol{\lambda}_t = \mathbf{0}$ and that the bilinear form can be expressed in the scalar valued normal component of the surface traction and the displacement. Moreover we assume that the actual contact zone and its discrete counterparts are compact subsets of Γ_c and that the discrete bilinear forms are equal to the continuous ones, and that no extra variational crime due to domain approximations enters. We refer to [6] for an analysis of a simple scalar valued linear mortar setting in case of curvilinear interfaces. From now on, $0 < c, C < \infty$ denote generic constants not depending on the mesh-size h.

We start by considering $\mathbf{M}(\boldsymbol{\lambda}_h)$ in more detail for the special case of $\nu = 0$. As in the continuous setting the solution dependent set $\mathbf{M}(\boldsymbol{\lambda}_h)$ reduces to a solution independent set $\mathbf{M}_h^+$ which is given by

$$\mathbf{M}_h^+ := \left\{ \boldsymbol{\mu}_h = \sum_{j=1}^{m_h^s} \beta_j \Psi_j \mathbf{n}_j,\ \beta_j \geq 0,\ j = 1, \ldots, m_h^s \right\}. \quad (8)$$

We point out that the discrete cone $\mathbf{M}_h^+$ is, in general, a non-conforming approximation of the contact pressure space. Even for the special case of a constant normal, the condition on β_j does, in general, not yield that $\mathbf{M}_h^+ \subset \mathbf{M}^+ := \{\boldsymbol{\mu} \in \mathbf{M},\ \boldsymbol{\mu}_t = \mathbf{0}, \langle \mu_n, w \rangle_{\Gamma_c} \geq 0,\ w \in W^+\}$ which is equal to $\mathbf{M}(\boldsymbol{\lambda})$ for $\nu = 0$. Moreover for a non-constant normal, we also do not find strongly that the tangential part $\boldsymbol{\mu}_h \mathbf{t}$ is equal to zero for a general $\boldsymbol{\mu}_h \in \mathbf{M}_h^+$.

Remark 1 Alternative choices to define $\mathbf{M}_h^+$ are

$$\mathbf{M}_{h;1}^+ := \mathbf{M}_h \cap \mathbf{M}^+, \quad (9a)$$

$$\mathbf{M}_{h;2}^+ := \left\{ \boldsymbol{\mu} \in \mathbf{M}_h, \boldsymbol{\beta}_i^{\mathbf{t}} = \mathbf{0}, \sum_{j=1}^{m_h^s} \int_{\Gamma_c} \beta_j^n \Psi_j \Phi_i \geq 0, \forall i \right\}, \quad (9b)$$

where $\{\Phi_l\}_{l=1,\ldots,m_h^s}$ is a set of suitable functions, e.g., standard nodal Lagrange elements. In the case of lowest order finite elements, most often, standard nodal hat functions or biorthogonal dual basis functions are taken as approximations. In the first case, we then have $\mathbf{M}_h^+ = \mathbf{M}_{h;1}^+ \subset \mathbf{M}_{h;2}^+$ if $\Phi_l = \Psi_l = N_l^{(1)}$. For $\Phi_l = N_l^{(1)}$ and biorthogonal basis functions Ψ_l, we find that $\mathbf{M}_{h;1}^+ \subset \mathbf{M}_h^+ = \mathbf{M}_{h;2}^+$. Here we do focus on the choice (8) but similar results can be obtained for (9a) and (9b).

We are interested in $\mathcal{O}(h^{t-1}), 2 < t < \frac{5}{2}$, a priori estimates, and thus we work with standard second order conforming finite elements for the displacement. For the Lagrange multiplier space $\mathbf{M}_h$, we consider different alternatives. At the moment we only require inf-sup stability and low order approximation properties. In addition to the discrete dual space $\mathbf{M}_h$, we use the scalar valued trace space W_h^s of V_h^s restricted to Γ_c.

Assumption 1 We assume that (M_h, W_h^s) satisfies a uniform inf-sup condition, that $\{\Psi_j\}_{j=1,\ldots m_h^s}$ forms a local partition of unity in the sense that

$$\sum_{j=1}^{m_h^s} \Psi_j = 1, \quad \text{supp } \Psi_j = \cup\{\overline{F} \in \mathcal{F}_h^s \text{ such that } x_j \in \overline{F}\},$$

that the number of nodes x_j per face is bounded independently of the mesh-size and that $\|\Psi_j\|_{0;\Gamma_c} = \mathcal{O}(h)$. Here $\mathcal{F}_h^s$ stands for the set of all faces of the slave side on the contact interface.

We note that (M_h, W_h^s) cannot satisfy an inf-sup condition if $m_h^s > n_h^s := \dim W_h^s$. Thus if Assumption 1 holds, we can find subspaces W_h of W_h^s such that (M_h, W_h) satisfies a uniform inf-sup condition and such that $m_h^s := \dim M_h = \dim W_h \leq \dim W_h^s$. We recall that if no inf-sup condition holds, the uniqueness of the Lagrange multiplier cannot be guaranteed. In terms of Assumption 1, we get a best approximation property of M_h, i.e., for $\mu \in H^s(\Gamma_c)$, $0 \leq s \leq 1$, we have

$$\inf_{\mu_h \in M_h} \left(\frac{\|\mu - \mu_h\|_{-\frac{1}{2};\Gamma_c}}{\sqrt{h}} + \|\mu - \mu_h\|_{0;\Gamma_c} \right) \leq C h^s |\mu|_{s;\Gamma_c}. \quad (10)$$

We note that a uniform inf-sup condition is standard for a saddle point analysis and many choices exist for M_h. Due to the inequality constraints on the Lagrange multiplier, we have to impose additional constraints on the basis functions of M_h.

To obtain optimal a priori estimates, we require the following assumptions to hold true. The non-conformity term in $\mathbf{u}_h$ can only be bounded if a sign condition on Ψ_j is imposed.

Assumption 2 Let $\{\Psi_j\}_{j=1,\ldots,m_h^s}$ be the basis of M_h defining $\mathbf{M}_h^+$ by (8). Then we assume that each basis has a positive mean value on the faces of its support, i.e., for all $j = 1, \ldots, m_h^s$, we have

$$\int_F \Psi_j > 0, \qquad F \in \mathcal{F}_h \text{ and } F \subset \text{supp } \Psi_j. \quad (11)$$

For the non-conformity term in $\boldsymbol{\lambda}_h$, we have to test the basis functions $\Psi_i, i = 1, \ldots, m_h^{\mathrm{s}}$, with the nodal basis functions $N_l^{(1)}$ of $W_h^{(1)}$. Here $W_h^{(1)}$ stands for the lowest order conforming finite element space associated with the slave mesh on Γ_{c}.

Assumption 3 Let $\{\Psi_j\}_{j=1,\ldots,m_h^{\mathrm{s}}}$ be the basis of M_h defining $\mathbf{M}_h^+$ by (8). Then we assume that each basis tested with $N_l^{(1)}$ has a non-negative integral value, i.e.,

$$\int_{\Gamma_{\mathrm{c}}} \Psi_j N_l^{(1)} \geq 0, \quad j = 1, \ldots, m_h^{\mathrm{s}}, \quad l = 1, \ldots, n_h^{\mathrm{s};(1)}, \quad (12)$$

where $n_h^{\mathrm{s};(1)}$ is the dimension of $W_h^{(1)}$.

These conditions on the basis functions of M_h can be easily verified and as we will see in Sect. 5 several choices exist. We note however that for $m_h^{\mathrm{s}} = n_h^{\mathrm{s}}$ and standard nodal basis functions for 20-node elements in 3D on hexahedrals (11) is not satisfied. In that case, the restriction to the faces yields 8-node elements on quadrilaterals, and on the reference square the basis function associated with the vertices have a negative mean value. We point out that if (12) is satisfied then we do automatically have $\int_{\Gamma_{\mathrm{c}}} \Psi_j \geq 0$ since $N_l^{(1)}$ form a partition of unity.

In addition to the assumptions on the Lagrange multiplier basis functions, we do need a regularity assumption on the shape of the actual contact zone $\Gamma_a \subset \Gamma_{\mathrm{c}}$ with $\overline{\Gamma}_a := \{x \in \Gamma_{\mathrm{c}},\ [u^n] = 0\}$.

Assumption 4 Let $\Sigma_{nh} := \{x \in \Gamma_{\mathrm{c}},\ \mathrm{dist}\,(x, \partial\Gamma_a) \leq nh\}, n = 2, 3$ and we assume that for $v \in H_0^{t-\frac{1}{2}}(\Gamma_{\mathrm{c}} \setminus \Gamma_a)$ it holds

$$\|v\|_{0;\Sigma_{nh}} \leq Ch^{t-\frac{1}{2}} |v|_{t-\frac{1}{2};\Gamma_{\mathrm{c}}}. \quad (13)$$

We note that (13) is naturally satisfied if the boundary of Γ_a is smooth enough, see e.g. [19], and that $[u^n]$ is in $H_0^{t-\frac{1}{2}}(\Gamma_{\mathrm{c}} \setminus \Gamma_a)$ if $\mathbf{u} \in \mathbf{H}^t(\Omega^{\mathrm{m}}) \times \mathbf{H}^t(\Omega^{\mathrm{s}})$.

Introducing the error $\mathbf{E}_h := (\mathbf{u} - \mathbf{u}_h, \boldsymbol{\lambda} - \boldsymbol{\lambda}_h)$ and its associated norm $E_h^2 := E_{\mathbf{u}}^2 + E_{\boldsymbol{\lambda}}^2 := \|\mathbf{u} - \mathbf{u}_h\|_{1;\Omega}^2 + \|\boldsymbol{\lambda} - \boldsymbol{\lambda}_h\|_{-\frac{1}{2};\Gamma_c}^2$, the standard saddle-point theory and the complementarity conditions provide a first upper bound for the error. The starting point for the a priori analysis is the following lemma, which has been introduced in [12] for standard Lagrange multipliers and no friction. We refer to [31] for an extension to friction.

Lemma 1 *Let* $(\mathbf{u}, \boldsymbol{\lambda})$ *be the weak solution of the simplified contact problem* (5) *and let* $(\mathbf{u}_h, \boldsymbol{\lambda}_h)$ *be the solution of the discrete formulation* (7) *with* $\nu = 0$. *If Assumption 1 holds, we then have*

$$cE_h^2 \leq \inf_{\mathbf{v}_h \in \mathbf{V}_h} \|\mathbf{u} - \mathbf{v}_h\|_{1;\Omega}^2 + \inf_{\boldsymbol{\mu}_h \in \mathbf{M}_h} \|\boldsymbol{\lambda} - \boldsymbol{\mu}_h\|_{-\frac{1}{2};\Gamma_c}^2 + b_n(\boldsymbol{\lambda}_h - \boldsymbol{\lambda}, \mathbf{u} - \mathbf{u}_h).$$

Proof For convenience, we recall the basic steps. Due to the special case, the equilibrium only involves the normal part of the Lagrange multiplier and $b_t(\boldsymbol{\lambda}, \mathbf{v}) = 0$ and $b_t(\boldsymbol{\lambda}_h, \mathbf{v}_h) = 0$. Firstly the uniform inf-sup stability of the discrete spaces and the continuity of $a(\cdot, \cdot)$ and $b_n(\cdot, \cdot)$ in combination with (5a) and (7a) yield

$$cE_{\boldsymbol{\lambda}} \leq \inf_{\boldsymbol{\mu}_h \in \mathbf{M}_h} \|\boldsymbol{\lambda} - \boldsymbol{\mu}_h\|_{-\frac{1}{2};\Gamma_{\mathrm{c}}} + \|\mathbf{u} - \mathbf{u}_h\|_{1;\Omega}.$$

Secondly, the coercivity of the bilinear form $a(\cdot, \cdot)$ and the continuity of $a(\cdot, \cdot)$ and $b_n(\cdot, \cdot)$ in combination with (5a) and (7a) gives

$$cE_{\mathbf{u}}^2 \leq b_n(\boldsymbol{\lambda} - \boldsymbol{\lambda}_h, \mathbf{u}_h - \mathbf{u}) + E_h \inf_{\mathbf{v}_h \in \mathbf{V}_h} \|\mathbf{u} - \mathbf{v}_h\|_{1;\Omega}.$$

Now in terms of Young's inequality the a priori result is obtained. □

We note that (5b) and (7b) did not enter into the proof and that the upper bound is independent of the definition of the convex cone $\mathbf{M}_h^+$. The first two terms in the upper bound of Lemma 1 are the best approximation errors and are standard for a saddle-point problem. They reflect the quality of the approximation property of the spaces $\mathbf{V}_h$ and $\mathbf{M}_h$ and yield, due to Assumption 1, see also (10), order h^{t-1} bounds if $\mathbf{u} \in \mathbf{H}^t(\Omega^{\mathrm{m}}) \times \mathbf{H}^t(\Omega^{\mathrm{s}}), 2 < t < \frac{5}{2}$. The third term is a consistency error related to the inequality. We recall that for standard linear saddle point equality problems, a Galerkin orthogonality is satisfied, and thus this third term can be bounded by the first two terms. Unfortunately this does not hold for contact problems. Using the complementarity conditions $b_n(\boldsymbol{\lambda}, \mathbf{u}) = 0 = b_n(\boldsymbol{\lambda}_h, \mathbf{u}_h)$, it is trivial to see that

$$b_n(\boldsymbol{\lambda}_h - \boldsymbol{\lambda}, \mathbf{u} - \mathbf{u}_h) = b_n(\boldsymbol{\lambda}_h, \mathbf{u}) + b_n(\boldsymbol{\lambda}, \mathbf{u}_h).$$

The term $\max(b_n(\boldsymbol{\lambda}, \mathbf{u}_h), 0)$ is equal to zero if the discrete displacement satisfies the non-penetration condition pointwise, and thus this term can be regarded as a measure for the penetration of the discrete displacement. We recall that $\mathbf{M}_h^+$ is not necessarily a subspace of $\mathbf{M}^+$. As a consequence the term $\max(b_n(\boldsymbol{\lambda}_h, \mathbf{u}), 0)$ can be greater than zero, and thus this term measures the non-conformity of $\boldsymbol{\lambda}_h \mathbf{n}$ with respect to the physical requirement of a positive contact pressure. In our special case of a constant normal, we find that the tangential component of $\boldsymbol{\lambda}_h$ is strongly zero and thus no extra term occurs. However in a more general case, the approximation of the normal and tangential components also has to be taken into account.

So far, no properties of $\mathbf{M}_h^+$ did enter and the only constraint on the pairing $\mathbf{V}_h$ and $\mathbf{M}_h$ is the inf-sup stability. Assumptions 2 and 3 provide sufficient conditions on $\mathbf{M}_h^+$ such that $b_n(\boldsymbol{\lambda}_h - \boldsymbol{\lambda}, \mathbf{u} - \mathbf{u}_h)$ is of order h^{t-1}. In contrast to earlier work on quadratic finite elements for contact [12,13], we may also adapt the basis for nodes on the slave side of the contact part, and we do consider also the case $m_h^{\mathrm{s}} < n_h^{\mathrm{s}}$, see [10,13,24,28] for numerical results.

Before we bound $b_n(\boldsymbol{\lambda} - \boldsymbol{\lambda}_h, \mathbf{u} - \mathbf{u}_h)$, we provide some preliminary results. For the normal components of the negative surface stress and the displacement, we use the notation $\lambda^n := \boldsymbol{\lambda}\mathbf{n}$, $\lambda_h^n := \boldsymbol{\lambda}_h\mathbf{n}$ and $u^n := \mathbf{u}\mathbf{n}$, $u_h^n := \mathbf{u}_h\mathbf{n}$. Of crucial importance for the proof is the following observation:

$$\int_{\Gamma_c} [u_h^n]\Psi_j \leq 0, \quad j = 1, \ldots, m_h^s \tag{14}$$

which results from the definition of $\mathbf{M}_h^+$ and (7b). We exploit this sign property to define an L^2-stable operator which maps $[u_h^n]$ onto a pointwise non-positive function. As a preliminary step, we introduce locally on each contact face on the slave side a biorthogonal set of linearly independent functions with respect to $\{\Psi_i\}_{i=1,\ldots,m_h^s}$. The scaling is done such that both Ψ_i and the biorthogonal function have the same positive mean value. From these face-wise defined local functions we build a global basis denoted by $\{\Theta_i\}_{i=1,\ldots,m_h^s}$ in the same way as $\{\Psi_i\}_{i=1,\ldots,m_h^s}$ is obtained from its local contributions. This gluing step is standard for classical finite element basis functions. We point out that by Assumption 1 the local Ψ_i form a face-wise partition of unity, and thus the local Θ_i also do. Since the gluing step is the same for both, the global Θ_i also form a partition of unity. Moreover, Θ_i is in general not continuous but, by construction, has the same support as Ψ_i and satisfies a global biorthogonality, i.e.,

$$\int_{\Gamma_c} \Psi_i\Theta_j = \delta_{ij}\int_{\Gamma_c} \Psi_i = \delta_{ij}\int_{\Gamma_c} \Theta_j. \tag{15}$$

In terms of $\{\Theta_i\}_{i=1,\ldots,m_h^s}$ we define two linear and L^2-stable operators Q_h and Q_h^*. Both operators can be locally evaluated $Q_h w := \sum_{j=1}^{m_h^s} \alpha_j\Theta_j \in M_h^* := \operatorname{span}\{\Theta_j, j = 1, \ldots, m_h^s\}$ and $Q_h^*\mu := \sum_{j=1}^{m_h^s} \beta_j\Psi_j \in M_h$ with α_j and β_j defined by

$$\alpha_j := \frac{\int_{\Gamma_c} w\Psi_j}{\int_{\Gamma_c} \Psi_j}, \quad \beta_j := \frac{\int_{\Gamma_c} \mu\Theta_j}{\int_{\Gamma_c} \Theta_j}, \quad j = 1, \ldots, m_h^s.$$

The operators have the following two important properties. Due to (15), we have the following orthogonality

$$\int_{\Gamma_c} Q_h^*\mu(w - Q_h w) = 0. \tag{16}$$

Stability and the fact that both basis sets $\{\Theta_i\}_{i=1,\ldots,m_h^s}$ and $\{\Psi_i\}_{i=1,\ldots,m_h^s}$ form a partition of unity guarantees a reproduction property of lowest order

$$\|w - Q_h w\|_{0;\Gamma_c} \leq Ch^s|w|_{s;\Gamma_c}, \; w \in H^s(\Gamma_c), 0 \leq s \leq 1, \tag{17a}$$

$$\|\mu - Q_h^*\mu\|_{0;\Gamma_c} \leq Ch^s|w|_{s;\Gamma_c}, \; w \in H^s(\Gamma_c), \; 0 \leq s \leq 1. \tag{17b}$$

We note that higher order reproduction properties can be true for special cases of $\{\Psi_i\}_{i=1,\ldots,m_h^s}$ but then additional assumptions have to be imposed.

Remark 2 If the sets $\{\Phi_i\}_{i=1,\ldots,m_h^s}$ and $\{\Psi_i\}_{i=1,\ldots,m_h^s}$ satisfy the biorthogonality relation

$$\int_F \Phi_j\Psi_i = \delta_{ij}\int_F \Phi_j, \quad i, j = 1, \ldots, m_h^s, \quad F \in \mathcal{F}_h,$$

then we have $\Phi_i = \Theta_i$ and thus $M_h^* = W_h$. Moreover due to the diagonal structure of the mass matrix, we obtain that Q_h is the mortar projection operator and Q_h^* its dual. Then (17a) also holds for $0 \leq s \leq 2$. However in the general setting, this does not hold true.

Remark 3 We point out that, in general, we cannot guarantee that $\Theta_i \geq 0$. Moreover, due to the biorthogonality (15), Θ_i and Ψ_i cannot be both non-negative for all indices. Of special interest are situations where one set of basis functions is non-negative but this is not a necessary condition and only simplifies the proof.

We note that the following lemma is an abstract version of a result in [12], see [13] for similar techniques and alternative spaces.

Lemma 2 *Under the regularity assumption of the solution* $\mathbf{u} \in \mathbf{H}^t(\Omega^m) \times \mathbf{H}^t(\Omega^s)$, $2 < t < \frac{5}{2}$, *and Assumption 2, we obtain for the consistency term in the displacement*

$$b_n(\boldsymbol{\lambda}, \mathbf{u}_h) \leq C\left(h^{2(t-1)}|\mathbf{u}|_{t;\Omega}^2 + h^{t-1}|\mathbf{u}|_{t;\Omega}\|\mathbf{u} - \mathbf{u}_h\|_{1;\Omega}\right)$$

provided that the actual contact region $\Gamma_a \subset \Gamma_c$ *satisfies* (13) *(Assumption 4).*

Proof We start with the construction of an operator P_h which maps $[u_h^n]$ onto a point-wise non-positive function. By Assumption 2 and by construction of Θ_j, we have that $a_j^F := \int_F \Theta_j = \int_F \Psi_j > 0$ for $F \subset \operatorname{supp}\Theta_j = \operatorname{supp}\Psi_j$. Now there are two possibilities: In the case that $\Theta_j \geq 0$, we set $P_h := Q_h$ otherwise we do use a sub-partitioning of Γ_c into non-overlapping simply connected shape regular boxes B_j such that the 2-dimensional area of $B_j \cap F$ is equal to a_j^F and such that the node x_j is in B_j. We recall that

$$\sum_{j=1}^{m_h^s} a_j^F = |F|, \quad \sum_{j=1}^{m_h^s}\sum_{F\in\mathcal{F}_h} a_j^F = |\Gamma_c|,$$

and thus such a partition can be easily found. Associated with each box B_j is now the characteristic function χ_j. Let $Q_h w = \sum_{j=1}^{m_h^s} \alpha_j\Theta_j$, then we define $P_h w := \sum_{j=1}^{m_h^s} \alpha_j\chi_j$, and due to (14), we get $P_h[u_h^n] \leq 0$ strongly. Observing

$\int_F \chi_j = \int_F \Theta_j$, we find in terms of (16)

$$\begin{aligned} b_n(\boldsymbol{\lambda}, \mathbf{u}_h) &= \langle \lambda^n, [u_h^n] - Q_h[u_h^n] + Q_h[u_h^n] \rangle_{\Gamma_c} \\ &= \langle \lambda^n - Q_h^* \lambda^n, [u_h^n] - Q_h[u_h^n] \rangle_{\Gamma_c} \\ &\quad + \langle \lambda^n, Q_h[u_h^n] - P_h[u_h^n] \rangle_{\Gamma_c} + \langle \lambda^n, P_h[u_h^n] \rangle_{\Gamma_c} \\ &\leq \langle \lambda^n - Q_h^* \lambda^n, [u_h^n] - Q_h[u_h^n] \rangle_{\Gamma_c} \\ &\quad + \langle \lambda^n, Q_h[u_h^n] - P_h[u_h^n] \rangle_{\Gamma_c} \\ &= \langle \lambda^n - Q_h^* \lambda^n, [u_h^n] - Q_h[u_h^n] \rangle_{\Gamma_c} \\ &\quad + \langle \lambda^n - \Pi_0 \lambda^n, Q_h[u_h^n] - P_h[u_h^n] \rangle_{\Gamma_c}, \end{aligned}$$

where Π_0 is the L^2-projection onto face-wise constants. The approximation properties (17) of Q_h^* and Q_h now allow us to bound the first term on the right. Using $s = \frac{1}{2}$ in (17a) and $0 < s = t - \frac{3}{2} < 1$ in (17b) and inserting $\pm[u^n], \pm Q_h[u^n]$, we get as bound

$$C\sqrt{h} h^{t-\frac{3}{2}} |\mathbf{u}|_{t;\Omega} E_{\mathbf{u}} + \langle \lambda^n - Q_h^* \lambda^n, [u^n] - Q_h[u^n] \rangle_{\Gamma_c}.$$

The second term on the right has a similar structure and can be bounded by

$$C\sqrt{h} h^{t-\frac{3}{2}} |\mathbf{u}|_{t;\Omega} E_{\mathbf{u}} + \langle \lambda^n - \Pi_0 \lambda^n, Q_h[u^n] - P_h[u^n] \rangle_{\Gamma_c}.$$

Here, we have also used the approximation property of Π_0 and of P_h. Adding these two bounds and using (16) and the definition of P_h, we get

$$b_n(\boldsymbol{\lambda}, \mathbf{u}_h) \leq C h^{t-1} |\mathbf{u}|_{t;\Omega} E_{\mathbf{u}} + \langle \lambda^n, [u^n] - P_h[u^n] \rangle_{\Gamma_c}.$$

In the last step, we exploit the complementarity and find in terms of the local L^2-stability of P_h and Q_h and Assumption 4

$$\begin{aligned} &\langle \lambda^n, [u^n] - P_h[u^n] \rangle_{\Gamma_c} = -\langle \lambda^n, P_h[u^n] \rangle_{\Gamma_c} \leq h^{t-\frac{3}{2}} |\mathbf{u}|_{1;\Omega} \\ &C \left(\|[u^n] - P_h[u^n]\|_{0;\Sigma_{2h}} + \|[u^n] - Q_h[u^n]\|_{0;\Sigma_{2h}} \right) \\ &\leq C h^{t-\frac{3}{2}} |\mathbf{u}|_{1;\Omega} \|[u^n]\|_{0;\Sigma_{3h}} \leq C h^{t-\frac{3}{2}} h^{t-\frac{1}{2}} |\mathbf{u}|_{1;\Omega}^2. \end{aligned}$$

□

We point out that if $P_h = Q_h$ and if $W_h^{(1)} \subset W_h = M_h^*$, the Assumption 4 is not required and we can directly use the bound

$$\|[u^n] - Q_h[u^n]\|_{0;\Gamma_c} \leq C h^{t-\frac{1}{2}} |[u^n]|_{t-\frac{1}{2};\Gamma_c}.$$

Lemma 3 *Under Assumption 3 and the regularity assumption* $\mathbf{u} \in \mathbf{H}^t(\Omega^m) \times \mathbf{H}^t(\Omega^s)$, $2 < t < \frac{5}{2}$, *we obtain for the consistency term in the contact pressure*

$$b_n(\boldsymbol{\lambda}_h, \mathbf{u}) \leq C h^{t-1} |\mathbf{u}|_{t;\Omega} \|\boldsymbol{\lambda} - \boldsymbol{\lambda}_h\|_{-\frac{1}{2};\Gamma_c}$$

provided that the actual contact region $\Gamma_a \subset \Gamma_c$ *satisfies* (13) *(Assumption 4).*

Proof Let $\tilde{S}_h$ be a locally defined Clément type operator onto $W_h^{(1)}$ being L^2-stable and of approximation order h^{t-1} with respect to the $H^{1/2}$-norm. Moreover $\tilde{S}_h w \leq 0$ for $w \leq 0$. The existence of such an operator is guaranteed, see e.g. [3,21]. It can be easily locally constructed. Each element in $W_h^{(1)}$ is uniquely defined by its values at the vertices p_j. Setting $\tilde{S}_h w(p_j)$ for all interior vertices on Γ_c as mean value of w on a ball K_j with center p_j and radius $\mathcal{O}(h)$ such that $K_j \subset \operatorname{supp} N_j^{(1)}$, we get $\tilde{S}_h w(p_j) \leq 0$ for $w \leq 0$ and $\tilde{S}_h w(p_j) = w(p_j)$ is w is affine on K_j. Having $\tilde{S}_h[u^n] = \sum_{j=1}^{n_h^{s,(1)}} \tilde{\beta}_j N_j^{(1)}$, we then define $S_h[u^n] := \sum_{j=1}^{n_h^{s,(1)}} \beta_j N_j^{(1)}$ with $\beta_j := \tilde{\beta}_j$ if $\operatorname{supp} N_j^{(1)} \subset \operatorname{supp}[u^n]$ and $\beta_j := 0$ otherwise. The definition of the coefficient gives that $\operatorname{supp} S_h[u^n] \subset \operatorname{supp}[u^n]$ and thus that $\langle \lambda^n, S_h[u^n] \rangle_{\Gamma_c} = 0$. The triangle inequality, an inverse estimate and the stability guarantee that $\|[u^n] - S_h[u^n]\|_{\frac{1}{2};\Gamma_c}$ can be bounded by

$$\|[u^n] - \tilde{S}_h[u^n]\|_{\frac{1}{2};\Gamma_c} + \frac{c}{\sqrt{h}} \|[u^n]\|_{0;\Sigma_h}.$$

Finally Assumption 4 and the approximation properties of $\tilde{S}_h$ yield

$$\|[u^n] - S_h[u^n]\|_{\frac{1}{2};\Gamma_c} \leq C h^{t-1} |[u^n]|_{t-\frac{1}{2};\Gamma_c}.$$

We observe that by construction $\beta_j \leq 0$ and $\lambda_h^n = \sum_{j=1}^{m_h^s} \gamma_j \Psi_j$ with $\gamma_j \geq 0$ and thus by Assumption 3, $\langle \lambda_h^n, S_h[u^n] \rangle_{\Gamma_c} = \sum_{j=1}^{m_h^s} \sum_{i=1}^{n_h^{s,(1)}} \gamma_j \beta_i \int_{\Gamma_c} \Psi_j N_i^{(1)} \leq 0$. Then in terms of the complementarity, we get

$$\begin{aligned} b_n(\boldsymbol{\lambda}_h, \mathbf{u}) &= \langle \lambda_h^n - \lambda^n, [u^n] \rangle_{\Gamma_c} \\ &= \langle \lambda_h^n - \lambda^n, [u^n] - S_h[u^n] \rangle_{\Gamma_c} + \langle \lambda_h^n, S_h[u^n] \rangle_{\Gamma_c} \\ &\leq \langle \lambda_h^n - \lambda^n, [u^n] - S_h[u^n] \rangle_{\Gamma_c} \\ &\leq \|\lambda^n - \lambda_h^n\|_{-\frac{1}{2};\Gamma_c} \|[u^n] - S_h[u^n]\|_{\frac{1}{2};\Gamma_c} \\ &\leq C h^{t-1} |\mathbf{u}|_{t;\Omega} \|\boldsymbol{\lambda} - \boldsymbol{\lambda}_h\|_{-\frac{1}{2};\Gamma_c}. \end{aligned}$$

□

5 Examples for the Lagrange multiplier basis

In this section, we present four choices of Lagrange multiplier basis functions such that Assumptions 1–3 are satisfied. The first two cases use nodal Lagrange basis functions of zero and first order and can be found in [10] and [28], respectively. The third and fourth choices are based on biorthogonality and are discussed in detail from the implementational and numerical point of view in [24]. We note that although Assumption 4 formally enters into Lemma 2 and into Lemma 3, it can be removed in special situations. But all our choices require in Lemma 2 or in Lemma 3 this assumption.

5.1 Zero order nodal Lagrange elements

The most natural possibility to define a Lagrange multiplier space is to set $\Psi_j := \chi_{F_j}$, where χ_{F_j} is the characteristic function of the face $F_j \in \mathcal{F}_h$. If this choice is used in combination with lowest order finite elements, no uniform inf-sup condition can be established and then as done in [10] a bubble enrichment stabilization is required. However, this choice in combination with 27-node hexahedral elements satisfies a uniform inf-sup condition and no further stabilization is required. Moreover, Assumptions 1–3 trivially hold. We note that this choice can only be applied for 27-node hexahedral elements, all other quadratic approaches require an additional stabilization.

5.2 First order nodal Lagrange elements

Another alternative is to set set $\Psi_j := N_j^{(1)}$, and thus we have $m_h^{\mathrm{s}} = n_h^{\mathrm{s};(1)} < n_h^{\mathrm{s}}$. Since Ψ_j is strictly positive in the interior of its support Assumptions 2 and 3 trivially hold. Assumption 1 is also satisfied since $(M_h, W_h^{(1)})$ is uniformly inf-sup stable and $W_h^{(1)} \subset W_h^{\mathrm{s}}$. We point out that for $m_h^{\mathrm{s}} < n_h^{\mathrm{s}}$ we obtain a rectangular coupling matrix. However a non-singular square matrix can be extracted. For this choice, we obtain $M_h^+ \subset M_h$ and thus Lemma 3 trivially holds, and moreover without any additional assumption we find $b_n(\boldsymbol{\lambda}_h, \mathbf{u}) \leq 0$. The only drawback of this choice is that this square matrix is a typical mass matrix and has a dense inverse.

5.3 First order biorthogonal Lagrange elements

To obtain a more local coupling between surface traction and displacement, we also propose dual Lagrange multiplier spaces resulting in a diagonal square matrix, after a possible basis transformation [24]. Here, we consider two choices. Firstly, we do take the biorthogonal basis functions well established in the lowest order case. Then the basis functions Ψ_j satisfy

$$\int_F \Psi_j N_l^{(1)} = \delta_{lj} \int_F N_l^{(1)}, \quad j,l = 1,\dots,n_h^{\mathrm{s};(1)}, F \in \mathcal{F}_h,$$

and thus Assumptions 1–3 hold.

5.4 Second order biorthogonal Lagrange elements

Secondly, we consider the situation $m_h^{\mathrm{s}} = n_h^{\mathrm{s}}$. As already pointed out a local biorthogonalization step of the nodal quadratic basis function results in basis function which do satisfy Assumption 1 but possibly violate Assumptions 2 and 3. Thus in a pre-process we transfer for simplicials and 20-node elements on hexahedrals the nodal basis functions of the displacements such that the newly defined basis functions Φ_j form face-wise a partition of unity and have a positive mean value. Let $\tilde{\Phi}_p$ and $\tilde{\Phi}_m$ be the standard nodal second order basis functions associated with the vertices and midpoints of the edges, respectively. Then we set $\Phi_p := \tilde{\Phi}_p + \frac{1}{5}\sum_{m\in\mathcal{M}_p} \tilde{\Phi}_m$ and $\Phi_m := \frac{3}{5}\tilde{\Phi}_m$. Here $\mathcal{M}_p$ is the set of all edge midpoints such that m and p are on a same edge. In the case of 27-node hexahedral elements, we use the standard nodal basis. Although the newly defined Φ_j are not strictly positive in the interior of the support, we observe that the mean values are positive. Moreover Φ_j form a partition of unity. Then we perform a local biorthogonalization step followed by an edge or vertex based gluing step to obtain the basis functions of M_h. By construction the resulting mass matrix is diagonal and of size $n_h^{\mathrm{s}} \times n_h^{\mathrm{s}}$. Moreover due to the biorthogonality condition, the Ψ_j form face-wise a partition of unity and have a positive mean value on each face which is part of the support [24]. Thus Assumptions 1 and 2 are guaranteed. We point out that just like the Φ_j, the Ψ_j are not strictly positive. To see that Assumption 3 is satisfied, it is sufficient to observe that $N_p^{(1)}$ can be written as a linear combination of the newly defined basis functions with non-negative coefficients. For this choice, the proof of Lemma 2 simplifies significantly. Noting $P_h = Q_h$ and that Q_h is the mortar projection, we get the bound

$$\begin{aligned} b_n(\boldsymbol{\lambda}, \mathbf{u}_h) &\leq \langle \lambda^n - Q_h^* \lambda^n, [u_h^n] - Q_h[u_h^n] \rangle_{\Gamma_c} \\ &\leq \|\lambda^n - Q_h^* \lambda^n\|_{-\frac{1}{2};\Gamma_c} \|[u_h^n] - Q_h[u_h^n]\|_{\frac{1}{2};\Gamma_c} \\ &\leq C h^{t-1} |\mathbf{u}|_{t;\Omega} \left(h^{t-1} |\mathbf{u}|_{t;\Omega} + \|\mathbf{u} - \mathbf{u}_h\|_{1;\Omega} \right). \end{aligned}$$

Here standard properties of the mortar projection such as $H^{1/2}$-stability and best approximation properties in combination with $W_h^{(1)} \subset M_h^*$ have been used.

6 Numerical results

Two numerical examples are presented to demonstrate the validity of the derived a priori estimates and the robustness of the resulting mortar approach for quadratic finite elements. For the sake of simplicity, we restrict our investigations to the last of the four cases considered in Sect. 5, i.e. locally quadratic biorthogonal Lagrange multiplier basis functions, and 20-node hexahedral finite elements. However, similar numerical studies focusing on the other three choices are readily found in the literature, see e.g. [10,28,24]. All given simulations are based on a parallel implementation of the proposed contact algorithms in our in-house multiphysics research code BACI [30].

Spatial convergence is analyzed for a Hertzian type contact problem with relatively small deformations in Sect. 6.1, whereas the more general framework of finite deformation contact and nonlinear material behavior is addressed with a

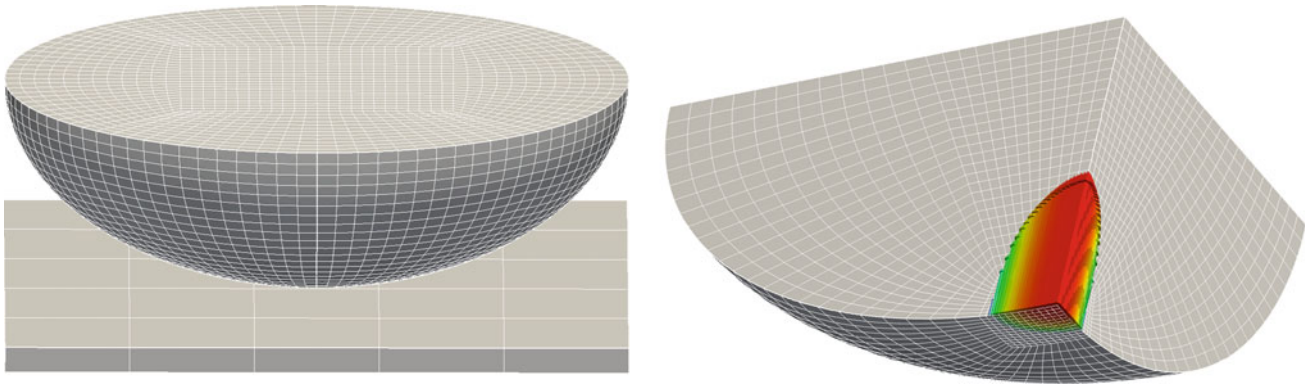

Fig. 1 Hertzian type contact—problem setup and exemplary finite element mesh (*left*), one quarter of deformed geometry and schematic normal contact traction solution (*right*)

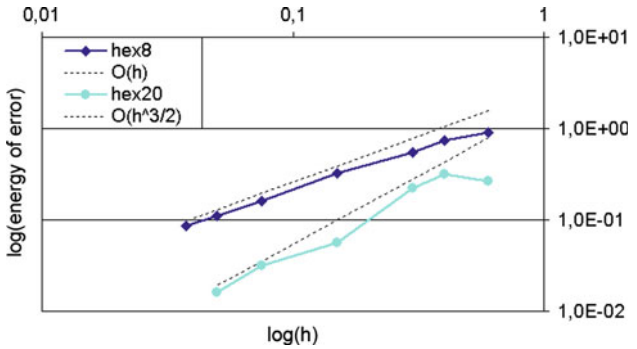

Fig. 2 Hertzian type contact—convergence of error in the energy norm with uniform mesh refinement for 8-node and 20-node hexahedral meshes using dual Lagrange multipliers

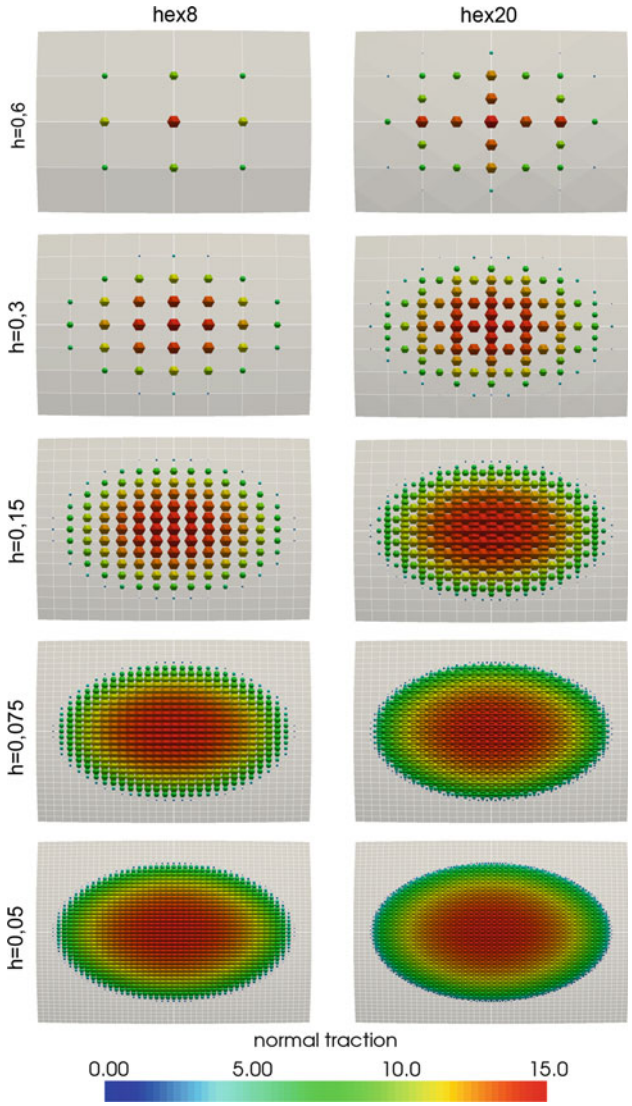

Fig. 3 Hertzian type contact—vertical closeup view of the active contact zone and visualization of the normal contact traction solution for different mesh sizes h using 8-node hexahedral elements (*left*) and 20-node hexahedral elements (*right*)

torus impact example in Sect. 6.2. Further results for quadratic finite elements, e.g. considering Coulomb friction and 27-node hexahedral elements, can also be found in [24]. We point out that our actual implementation is always fully nonlinear (i.e. based on a nonlinear measure of strain) and thus takes into account the effect of geometrical nonlinearity. Important algorithmic aspects in this regard are a consistent linearization of all contact terms and the introduction of an efficient semi-smooth Newton type active set strategy. For all details concerning these two topics, the interested reader in referred to our previous work [15,22,23,31].

6.1 Small deformations: Hertzian type contact

As a first validation step, we analyze a 3D Hertzian type contact problem which consists of an elastic half-ellipsoid ($R_1 = 12$, $R_2 = R_3 = 8$, St. Venant–Kirchhoff material model with Young's modulus $E = 200$, Poisson's ratio $\nu = 0.3$) and a rigid planar surface. Contact interaction is assumed to be frictionless and a constant pressure $p = 0.2$ is applied to the top surface of the elastic body. The problem setup, an exemplary

finite element mesh and an exemplary numerical solution for the normal contact traction are visualized in Fig. 1.

Mortar finite element discretization is based on first-order (*hex8*) and second-order (*hex20*) hexahedral elements in combination with dual Lagrange multipliers, see Sect. 5.4. The convergence study carried out in the following analyzes the discretization error $\mathbf{u} - \mathbf{u}_h$ in the energy norm, which is defined as

$$\|\mathbf{u} - \mathbf{u}_h\|_{energy} = \sqrt{\int_{\Omega} (\boldsymbol{\epsilon} - \boldsymbol{\epsilon}_h) : \mathbb{C} : (\boldsymbol{\epsilon} - \boldsymbol{\epsilon}_h)\, \mathrm{d}\Omega}. \qquad (18)$$

While an analytical solution for the contact tractions is readily available for Hertzian type problems [29], no such solutions exist for the displacements in the contacting bodies. Therefore, to evaluate the discretization error, we compute a reference solution $\mathbf{u}_{ref}$ corresponding to a very fine *hex20* mesh. The results of our convergence study are summarized in Fig. 2. It can be seen very clearly that both the linear case and the quadratic case are in perfect accordance with what can be expected from the a priori error estimates. Especially the $\mathcal{O}(h^{3/2})$ result for the *hex20* discretization with dual Lagrange multipliers demonstrates the appeal of quadratic mortar finite elements for contact problems. Provided that the solution is regular enough, a considerable qualitative gain in accuracy as compared with first-order interpolation can be achieved.

Numerical results for the active contact zone and for the normal contact traction distribution are illustrated in Fig. 3 for first-order interpolation and second-order interpolation with different mesh sizes h, respectively. Both the elliptical shape of the contact zone and the parabolic traction profile are resolved more and more with mesh refinement. While Fig. 3, in contrast to the convergence study presented above, does not allow for a real quantification of results, it at least visually confirms the high accuracy obtainable with mortar finite elements in general and with the proposed quadratic version in particular.

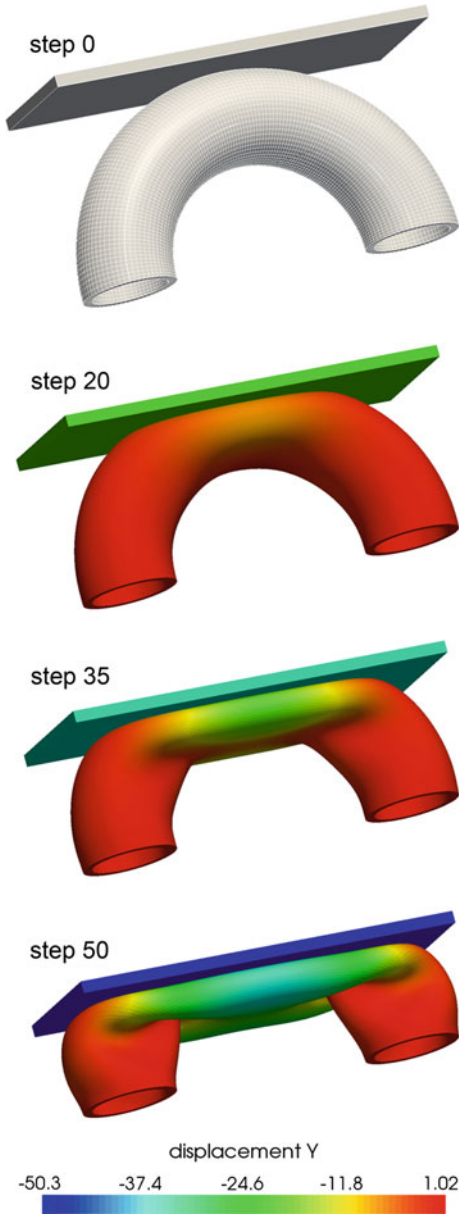

Fig. 5 Torus impact—finite element mesh and characteristic stages of deformation

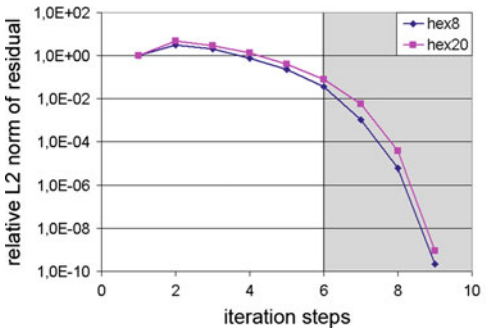

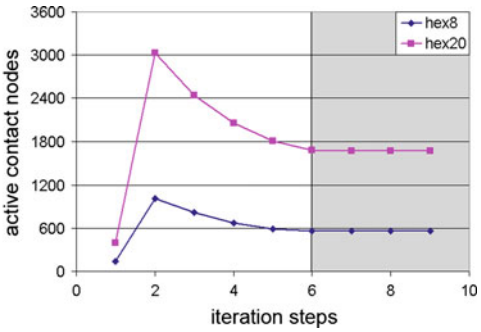

Fig. 4 Hertzian type contact—exemplary convergence behavior of the semi-smooth Newton method in terms of the relative L^2-norm of the residual (*left*) and in terms of the active contact set (*right*) for a mesh size of $h = 0.075$. The shaded regions indicate that the active contact set is already fully converged within these iteration steps

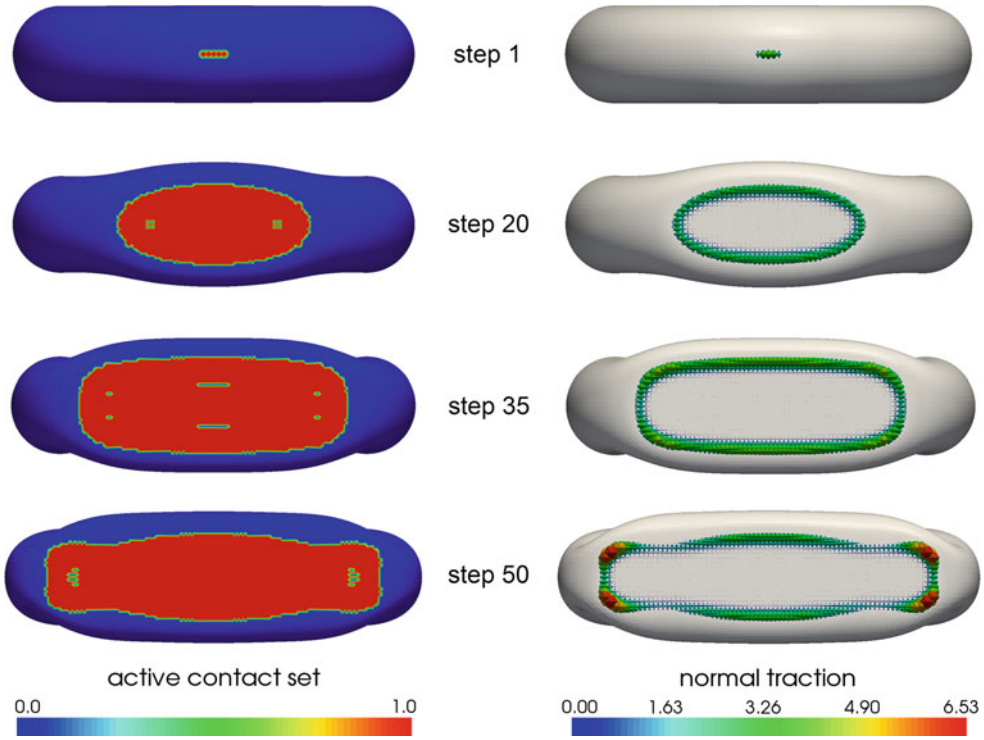

Fig. 6 Torus impact—*top view* of the torus structure with visualization of the active contact set (*left*, 1 = active) and of the normal contact traction solution (*right*)

It is worth mentioning that only relatively small deformations occur in the given example and thus a numerical procedure based on linearized kinematics as introduced in Sect. 2 would already yield quite accurate solutions. Nevertheless, as mentioned before, our actual implementation here is fully nonlinear. The results concerning numerical efficiency of the employed semi-smooth Newton type active set strategy [15,22,23] are given in Fig. 4. For an exemplary finite element mesh, we monitor the relative L^2-norm of the total residual and the number of active nodes over all nonlinear iteration steps of the single load step needed to solve the presented Hertzian type contact example. Regardless of the interpolation order, the semi-smooth Newton approach locates the correct active set (which consists of up to 1669 nodes here) within only a few iteration steps. With the active set being fixed, the nonlinear iteration scheme reduces to a standard (smooth) Newton method, and thus we obtain quadratic convergence in the limit owing to the underlying consistent linearization [22,23].

6.2 Finite deformations: Torus impact

The second example illustrates the robustness of the dual quadratic mortar finite elements proposed in [24] and reviewed in Sect. 5.4 in the more general case of finite deformation contact with siginificant active set changes. The considered test setup consists of a hollow half-torus (Neo–Hookean material model with Young's modulus $E = 100$, Poisson's ratio $\nu = 0.3$) and a rigid planar surface. The major and minor radii of the half-torus are 76 and 24, respectively, and the wall thickness is 4.5. The bottom surfaces of the half-torus are completely fixed, and an impact situation is generated by moving the rigid wall towards the elastic body with a prescribed displacement $u = 50$ accumulated over 50 quasi-static load steps. Figure 5 shows the employed finite element mesh consisting of 20-node hexahedral elements (with 50,720 nodes in total) as well as some characteristic stages of deformation. Shortly after the final step shown here, self contact occurs on the inside of the hollow torus, which is beyond the scope of the present contribution.

The evolution of active contact zone and contact traction distribution can be tracked in Fig. 6. Particularly interesting here is the fact that, while the actual load transfer is mainly restricted to a narrow region close to the boundary of the contact zone, the inner part of the contact zone nevertheless remains almost entirely active. Considering the typical structure of the non-penetration conditions in (2), where *either* the normal gap *or* the normal contact traction is forced to zero, the given situation can be considered extremely challenging for the employed active set strategy. However, as Table 1 exemplarily confirms for one representative load step, our semi-smooth Newton type active

Table 1 Torus impact—convergence behavior of the semi-smooth Newton method in terms of the relative L^2-norm of the total residual for a representative load step

Step	Relative L^2-norm of residual
1	7.31e+01[a]
2	6.67e+01[a]
3	3.54e+01[a]
4	8.16e+00[a]
5	4.76e−01
6	8.34e−05
7	9.66e−09

[a] Change in active contact set

set strategy [22,23] does not have any problems with the described situation, but resolves all nonlinearities (including the search for the correct active set) within only a few Newton steps. Again, owing to the underlying consistent linearization, quadratic convergence is obtained in the limit.

7 Conclusions

In this paper, a variationally consistent contact formulation in terms of quadratic mortar finite element methods has been considered and a novel abstract framework for the a priori error analysis has been established. As the main theoretical result, it has been shown that under quite weak assumptions on the discrete Lagrange multiplier space $\mathcal{O}(h^{t-1}), 2 < t < \frac{5}{2}$, a priori estimates can be obtained. Numerical investigations for one particularly promising type of Lagrange multiplier interpolation (second-order biorthogonal basis functions) fully confirm the theoretical results. Besides the optimal spatial convergence properties of the resulting second-order mortar approach, its robustness in the context of finite deformations using a semi-smooth Newton type active set strategy has also been demonstrated.

Both the theoretical and the numerical results presented in this contribution certify that quadratic mortar finite elements may offer a considerable qualitative gain for contact problems as compared with first-order interpolation provided that the solution is regular enough. Future work should aim at exploiting this advantage to the full extent wherever appropriate.

References

1. Alart P, Curnier A (1991) A mixed formulation for frictional contact problems prone to Newton like solution methods. Comput Methods Appl Mech Eng 92:353–375
2. Belhachmi Z, Ben Belgacem F (2003) Quadratic finite element approximation of the Signorini problem. Math Comput 72:83–104
3. Chen Z, Nochetto R (2000) Residual type a posteriori error estimates for elliptic obstacle problems. Numer Math 84:527–548
4. Eck C, Jarusek J, Krbec M (2005) Unilateral contact problems: variational methods and existence theorems. Chapman & Hall/CRC, Boca Raton
5. Fischer-Cripps A (2000) Introduction to contact mechanics, mechanical engineering series. Springer, New York
6. Flemisch B, Melenk J, Wohlmuth BI (2005) Mortar methods with curved interfaces. Appl Numer Math 54:339–361
7. Gitterle M, Popp A, Gee MW, Wall WA (2010) Finite deformation frictional mortar contact using a semi-smooth Newton method with consistent linearization. Int J Numer Methods Eng 84:543–571
8. Hager C, Wohlmuth BI (2010) Semismooth Newton methods for variational problems with inequality constraints. GAMM Mitteilungen 33:8–24
9. Han W, Sofonea M (2002) Quasistatic contact problems in viscoelasticity and viscoplasticity, Studies in Advanced Mathematics, American Mathematical Society. International Press, Somerville
10. Hauret P, Le Tallec P (2007) A discontinuous stabilized mortar method for general 3d elastic problems. Comput Methods Appl Mech Eng 196:4881–4900
11. Hertz H (1882) Über die Berührung fester elastischer Körper. J Reine Angew Math 92:156–171
12. Hild P, Laborde P (2002) Quadratic finite element methods for unilateral contact problems. Appl Numer Math 41:410–421
13. Hüeber S, Mair M, Wohlmuth BI (2005) A priori error estimates and an inexact primal-dual active set strategy for linear and quadratic finite elements applied to multibody contact problems. Appl Numer Math 54:555–576
14. Hüeber S, Stadler G, Wohlmuth BI (2008) A primal-dual active set algorithm for three-dimensional contact problems with Coulomb friction. SIAM J Sci Comput 30:572–596
15. Hüeber S, Wohlmuth BI (2005) A primal-dual active set strategy for non-linear multibody contact problems. Comput Methods Appl Mech Eng 194:3147–3166
16. Johnson K (1985) Contact mechanics. Cambridge University Press, Cambridge
17. Kikuchi N, Oden JT (1988) Contact problems in elasticity: a study of variational inequalities and finite element methods. Society for Industrial and Applied Mathematics (SIAM), Philadelphia
18. Laursen TA (2002) Computational contact and impact mechanics. Springer, Berlin
19. Li J, Melenk J, Wohlmuth BI, Zou J (2010) Optimal a priori estimates for higher order finite elements for elliptic interface problems. Appl Numer Math 60:19–37
20. Moussaoui M, Khodja K (1992) Régularité des solutions d'un problème mêlé Dirichlet–Signorini dans un domaine polygonal plan. Commun Partial Differ Equ 17:805–826
21. Nochetto R, Wahlbin L (2002) Positivity preserving finite element approximation. Math Comput 71:1405–1419
22. Popp A, Gee MW, Wall WA (2009) A finite deformation mortar contact formulation using a primal-dual active set strategy. Int J Numer Methods Eng 79:1354–1391
23. Popp A, Gitterle M, Gee MW, Wall WA (2010) A dual mortar approach for 3D finite deformation contact with consistent linearization. Int J Numer Methods Eng 83:1428–1465
24. Popp A, Wohlmuth BI, Gee MW, Wall WA (2011) Dual quadratic mortar finite element methods for 3D finite deformation contact. Tech. report, Technische Universität München
25. Puso MA, Laursen TA (2002) A 3D contact smoothing method using Gregory patches. Int J Numer Methods Eng 54:1161–1194
26. Puso MA, Laursen TA (2004) A mortar segment-to-segment contact method for large deformation solid mechanics. Comput Methods Appl Mech Eng 193:601–629

27. Puso MA, Laursen TA (2004) A mortar segment-to-segment frictional contact method for large deformations. Comput Methods Appl Mech Eng 193:4891–4913
28. Puso MA, Laursen TA, Solberg J (2008) A segment-to-segment mortar contact method for quadratic elements and large deformations. Comput Methods Appl Mech Eng 197:555–566
29. Timoshenko SP, Goodier JN (1970) Theory of elasticity. McGraw-Hill, New York
30. Wall WA, Gee MW (2010) Baci—a multiphysics simulation environment. Tech. report, Technische Universität München
31. Wohlmuth BI (2011) Variationally consistent discretization schemes and numerical algorithms for contact problems. Acta Numerica, pp 569–734
32. Wriggers P (2002) Computational contact mechanics. Wiley, New York
33. Wriggers P, Nackenhorst U (eds) (2007) Computational methods in contact mechanics, vol 3 of IUTAM Bookseries. Springer, Berlin